Monometallic and bimetallic catalysts based on Pd, Cu and Ni for hydrogen transfer deoxygenation of a prototypical fatty acid to diesel range hydrocarbons

Kin Wai Cheah[1,2], Martin J. Taylor[1,3], Amin Osatiashtiani[1], Simon K. Beaumont[5], Daniel J. Nowakowski[1,4], Suzana Yusup[2]*, Anthony V. Bridgwater[1] and Georgios Kyriakou[1,4]*

[1] European Bioenergy Research Institute, Aston University, Aston Triangle, Birmingham, B4 7ET, United Kingdom

[2] Biomass Processing Centre, Centre of Biofuel and Biochemical Research, Institute of Self-Sustaining Building, Chemical Engineering Department, Universiti Teknologi PETRONAS, 32610, Seri Iskandar, Perak, Malaysia.

[3] Energy and Environment Institute and Department of Chemical Engineering, University of Hull, Cottingham Road, Hull, HU6 7RX, United Kingdom

[4] Chemical Engineering and Applied Chemistry, Aston University, Aston Triangle, Birmingham, B4 7ET, United Kingdom

[5] Department of Chemistry, Durham University, South Road, Durham, DH1 3LE, United Kingdom

* Corresponding authors:
g.kyriakou@aston.ac.uk (Georgios Kyriakou), drsuzana_yusuf@utp.edu.my (Suzana Yusup)

Graphical abstract

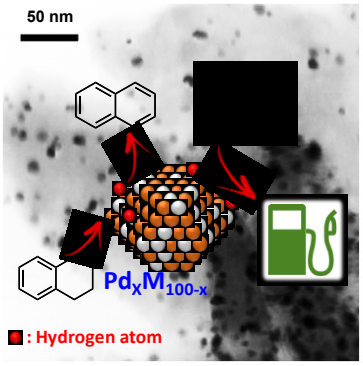

Abstract

Bimetallic $Pd_xNi_{(100-x)}$ and $Pd_xCu_{(100-x)}$ structures of a wide compositional range supported on activated carbon were synthesised via a simple, cheap and commercially relevant method. The surface and bulk properties of both the bimetallic structures and their monometallic counterparts were determined via STEM-EDS, TEM, XPS, powder XRD, N_2 porosimetry and ICP-OES. A close correlation between the XRD patterns and EDS elemental composition mapping of individual metal particles established the extent of palladium-base metal interaction in each sample. The performance of the different structures as catalysts for the selective hydrogenation and hydrodeoxygenation of oleic acid, a prototypical fatty acid, was evaluated using tetralin as a hydrogen donor. Catalysts displaying true bimetallic/alloy formation were found to improve the conversion of tetralin as compared to catalysts in which compositional segregation was observed. The $Pd_xNi_{(100-x)}$ series was found to outperform the $Pd_xCu_{(100-x)}$ catalysts in terms of hydrogen production via the dehydrogenation of tetralin, mirroring the fact that compositional segregation occurs more for the $Pd_xCu_{(100-x)}$ series than $Pd_xNi_{(100-x)}$. The hydrogen transfer deoxygenation of oleic acid over the monometallic and bimetallic catalysts was found to mirror the availability of hydrogen with those catalysts liberating more hydrogen also favouring the formation of C_{17} and C_{18} alkanes.

Keywords: Diesel; STEM-EDS; Palladium; Nickel; Copper; Bimetallic.

Introduction

To date, catalytic hydroprocessing technologies have advanced substantially with numerous technical breakthroughs and innovations. The catalytic hydrodeoxygenation of natural triglycerides using sulfided molybdenum catalysts on alumina supports with nickel and cobalt as the active metals has been well-studied in the literature.[1-5] It is an established technology that is used extensively for lipid biomass conversion to 'drop in' replacements for petroleum-derived transportation fuels. One major drawback in using bimetallic sulfided catalysts is the inherent need for an external sulfiding agent such as carbon disulfide (CS_2) or dimethyl disulfide (DMDS) in the liquid feed to maintain its catalytic activity. Moreover, sulfur leaching from the catalyst surface leads to a gradual decline in catalytic activity and eventual sulfur contamination of the liquid products. As a result, the strong dependency of sulphide-based catalysts on external sulfur agents has attracted considerable criticism in renewable fuel production as it incurs additional production costs and potentially adversely affects environment quality.[6]

More recently, there have been substantial efforts to design, formulate and develop non sulfide-based catalysts. Snåre et al.[7] screened a series of metal supported catalysts (Mo, Pd, Pt, Ir, Ru, Rh, and Os) on two different types of supports, metal oxides (including SiO_2, Al_2O_3, Cr_2O_3 and MgO) and activated carbon in a semi-batch deoxygenation system. Among the noble metal candidates, palladium has shown to be both highly active and selective in forming straight chain paraffinic hydrocarbons. Despite its superior catalytic performance, the high cost of noble metal based catalysts has hindered their large-scale industrial application. Furthermore, previous studies have reported that palladium as the active metal site is more susceptible to deactivation due to active site poisoning by adsorbed reaction intermediates such as heavy organic substances, carbonaceous deposits and carbon monoxide. This results in the rapid activity degradation of pure Pd nanomaterials, which further hinders its practical applicability in catalytic hydroprocessing.[8, 9] The vulnerability of Pd-based catalysts and their tendency for rapid deactivation, as well as their uneconomical application in large scale hydroprocessing, have stimulated further research to identify alternative materials that are suitable for this type of chemistry. This involves the development of non-noble based catalysts such as metal carbides, metal nitrides and metal phosphides supported catalysts for the deoxygenation of natural triglycerides and model compounds.[10, 11] All these emerging catalysts have demonstrated superior catalytic performances and high selectivity in producing hydrocarbons compared to sulfide-based and platinum group metal (PGM) based supported catalysts.

However, preparation of these catalysts is complicated and expensive as synthesis procedures often involve multi-step processes and lengthy synthetic protocols, thus hindering the large scale production of these materials.

Combining noble metals with an additional, cheaper metal is an effective low-cost, scalable substitute, which benefits from synergistic catalytic effects (geometric and electronic) between the two metals and decreased precious metal loadings. Pd-Ni and Pd-Cu bimetallic catalysts have been studied extensively for many applications including: alcohol oxidation, hydrogen separation, nitrate decomposition and electrochemical sensing.[12] The use of bimetallic systems for the catalytic deoxygenation of fatty acid molecules has received increased attention over the past years.[13, 14] Herein, we report a new strategy for the production of synthetic diesel like hydrocarbons using Pd-Ni and Pd-Cu bimetallic catalysts and tetralin (1,2,3,4-tetrahydronaphthalene). Tetralin was used as a hydrogen donor solvent in the reaction investigated in this study. The main reason for this choice is that the use of tetralin avoids the necessity to operate high pressure reactors with molecular hydrogen. Additionally, its excellent solubility in carboxylic acids suits this reaction very well. Moreover, hydrocarbon compounds like decalin and tetralin are usually used as hydrogen donors as well as stabilizing agent in fuel processing. Primary products of fuel processing are stabilised through transfer hydrogenation using these H-donors. Furthermore, Pd-based catalysts are known to be effective for the dehydrogenation of tetralin.[15]

The three metals used in this study (Pd, Ni and Cu) are well known as excellent catalysts for a wide range of hydrogenation reactions such as upgrading biomass-derived oxygenates,[16] CO_2 hydrogenation,[17] and the hydrogenation of stearic acid.[18, 19] Furthermore, replacing some of the Pd content in a hydrogenation catalyst offers the opportunity to reduce both the catalyst and process cost. Pd-Ni and Pd-Cu have been studied in the past for a variety of reactions including the hydrogenation of styrene and acetylene.[20] In order to be able to unequivocally attribute improvements in catalytic performance to the Pd-base metal synergism, monometallic supported equivalents of Pd_{100}, Ni_{100} and Cu_{100} were prepared at a nominal loading of 5 wt.% and the respective deoxygenation performances were evaluated. The individual roles of Pd, Ni and Cu metal catalysts in the deoxygenation of an unsaturated fatty acid model compound, oleic acid, to diesel like hydrocarbons were elucidated. Furthermore, a series of bimetallic Pd-Ni and Pd-Cu catalysts with different Pd:Ni and Pd:Cu molar ratios were synthesised in order to ascertain the presence of a promoting effect during the catalytic deoxygenation reactions.

Paraffinic diesel hydrocarbon selectivity was determined with various metal ratios, to determine the role of each component in the reaction. Lastly, the overall reaction pathways for the conversion of oleic acid and tetralin were proposed based on the product distribution of monometallic and bimetallic catalysts in different metal compositions.

Experimental

Materials and chemicals

The following chemicals were commercially available and used as received: Norit® D10 activated carbon powder (Alfa Aesar), oleic acid ($C_{18}H_{34}O_2$, 90%, Sigma-Aldrich), tetralin (1,2,3,4-tetrahydronaphthalene $C_{10}H_{12}$, anhydrous 99%, Sigma-Aldrich), copper (II) nitrate trihydrate ($Cu(NO_3)_2.3H_2O$ 99%, Acros Organics), nickel (II) nitrate hexahydrate ($Ni(NO_3)_2.6H_2O$, 98%, Alfa Aesar), tetramminepalladium (II) nitrate ($Pd(NH_3)_4(NO_3)_2$, 99.9%, Pd 5 wt.%, Alfa Aesar) and mesitylene (C_9H_{12}, 99%, Fluka) was used as the external standard. Deionised water was prepared in house. All gases such as hydrogen, nitrogen and helium were purchased in ultra-high purity (99.999%). All GC hydrocarbon standards (n-heptadecane, 1-heptadecene, n-octadecane, 1-octadecene, tetralin, oleic acid, stearic acid) were purchased from Sigma Aldrich and used as received.

Catalyst preparation

A series of activated carbon supported Pd, Cu, Ni, $Pd_xCu_{(100-x)}$ and $Pd_xNi_{(100-x)}$ catalysts were prepared via incipient wetness impregnation (IWI). The nominal metal loading of all catalysts synthesised was kept constant at 5 wt. %. Three types of monometallic catalysts Pd/C, Ni/C and Cu/C were prepared to serve as control materials. In a typical synthesis of Pd/C, Ni/C and Cu/C catalysts, mesoporous activated carbon Norit® D10 (0.95 g) was impregnated with the appropriate amount of aqueous metal salts of $Pd(NH_3)_4(NO_3)_2$, $Ni(NO_3)_2.6H_2O$ and $Cu(NO_3)_2.3H_2O$. Before adding the saturated solutions of corresponding metal salts to the bare support, the solutions were sonicated in a water bath for 0.5 h to ensure complete dissolution. After sonication, the solutions of corresponding metal salts were dispersed onto the support under continuous stirring at room temperature for 2 h before heating to 80 °C and aging for 24 h. Subsequently, the catalyst slurries were collected and annealed under flowing helium at 500 °C for 2 h and thereafter reduced under flowing hydrogen at 450 °C for 2 h. Bimetallic catalysts with different molar ratios of Pd-Cu and Pd-Ni were denoted as $Pd_xCu_{(100-x)}$ and $Pd_xNi_{(100-x)}$ respectively, where x is the molar percentage of Pd metal on the support and fixed at 20%, 40% and 60%. All compositions of Pd-Cu and Pd-Ni catalysts were prepared by a

similar method. The precursor solution mixtures were prepared by dissolving the appropriate amount of $Pd(NH_3)_4(NO_3)_2$ solution and $Ni(NO_3)_2.6H_2O$ or $Cu(NO_3)_2.3H_2O$ in 10 ml of deionised water to saturate the pores of the activated carbon support.

Catalyst characterisation

Surface areas and pore sizes were measured by N_2 physisorption on a Quantachrome Nova 4000 instrument, after sample outgassing at 120 °C for 4 h prior to analysis at -196 °C. Surface areas were calculated using the Brunauer–Emmett–Teller (BET) method over the range P/P_0 = 0.03–0.18, where a linear relationship was maintained. Pore size distributions were calculated using the Barrett–Joyner–Halenda (BJH) model applied to the desorption branch of the isotherm. Phase identification was evaluated by means of wide angle powder X-ray diffraction (XRD) on a Bruker D8 Advance diffractometer using the Cu Kα in the range 2θ = 10-80° with a step size of 0.04°. The crystallite size of the monometallic catalysts were estimated using the Scherrer equation applying to diffraction peaks at 46.3°, 42.9 and 44° for Pd, Cu and Ni particles respectively. X-ray Photoelectron Spectroscopy (XPS) measurements were conducted on a Kratos AXIS Supra employing a monochromated Al Kα X-ray source (hv = 1486.7 eV). Spectral fitting was performed using CasaXPS version 2.3.14, with binding energies corrected to the C 1s peak at 284.6 eV. Elemental analysis was performed using a Thermo Scientific iCAP 7000 series ICP-OES. Samples were prepared using ~10 mg of the catalyst, 100 mg ammonium fluoride (Sigma-Aldrich), 5 ml HNO_3 (68%, VWR Chemicals), 2 ml H_2SO_4 (>95%, Fisher), and 2 ml of deionised water. The mixture was stirred and digested for 0.5 h at 175 °C using a CEM Discover-S microwave system. Subsequently, the reactively-formed HF was neutralised using with 1 ml HCl (37%, VWR Chemicals) and 1 ml of boric acid solution (4%, Fluka). Finally, the samples were diluted 10 times with deionised water before being analysed on ICP-OES. Transmission electron microscopy (TEM) was performed using a JEOL 2100F FEG TEM operated at 200 kV in either bright field or scanning TEM modes, STEM-EDS was obtained using a JEOL dark field detector and Gatan bright field detector (latter at the entrance aperture for the Gatan Tridiem spectrometer). We estimated the convergence angle to be ~15 mrad. As the probe would be aberration limited during the STEM-EDS measurements the region probed during each measurement were estimated to be 3-4 nm. The instrument contains a high resolution pole piece with 1.0 mm Cs giving 2.3 Å point resolution and 1.0 Å imaging information limit. Samples were prepared by grinding to a fine powder, dispersion in ethanol (HPLC grade) by sonication and drop casting onto either holey carbon coated Cu or Ni grids (300 mesh, EM resolutions, grid metal selected to avoid interference with EDS signal being

measured), before evaporating to dryness under a warm lamp. For TEM imaging, images were acquired from at least 6 areas of the grid and particle size distributions were obtained by measuring the particle size using ImageJ software. Particle sizes obtained are for metallic (phase contrasting) particles and therefore STEM-EDS was undertaken to provide further insight into the extent of the bimetallic character of the particles. For the EDS measurements the probe was moved to the individual particles seen in the STEM images and the spectra acquired fitted using the areas under Gaussian peaks at 2.83, 7.47 and 8.05 keV, corresponding to the Pd Lα1, Ni Kα1 and Cu Kα1 transitions respectively.[21] Care was taken to ensure no overlapping signal of the Ni Kβ1 was present that could interfere with the Cu Kα1 measurement. The intensity ratios were calibrated by also measuring spectra acquired over a large area of the sample for each sample and referencing to the known metal contents obtained by ICP-OES. This approach gave a consistent calibration over multiple samples and was used to calibrate the axes of the frequency-composition plots shown. Each frequency-composition plot shows at least 50 particles measured individually in several areas of the grid. Examples of the STEM images and corresponding EDS measurements for the $Pd_{50}Ni_{50}$ sample are shown in the supporting information.

Catalytic tests

The hydrogenation and selective catalytic deoxygenation of oleic acid was performed in a mini autoclave reactor (Parr Instrument, 10 ml) operating in batch mode. A typical experiment was carried out as follows: oleic acid (1 ml; 3.17 mmol), tetralin (1 ml; 7.34 mmol) and catalyst (0.05 g) were charged into the autoclave reactor. Excess tetralin was used to ensure that the reaction takes place in excess hydrogen. The reactor was then purged with N_2 at ambient temperature for 10 min and the pressure was subsequently adjusted to 10 bar using the inert gas prior to the reaction. The reactor was then heated from room temperature to 330 ºC where it was kept constant for 3 h. These conditions were found to be optimal for this reaction in previous work.[22] Note that at these reaction conditions, all the reactants and products remain in the liquid/gas phase. Upon cooling down the reactor, the in-situ formed naphthalene from the dehydrogenation of tetralin, will solidify at temperatures < 80 °C which can facilitate the separation of naphthalene. The stirring speed was kept constant at 1100 rpm during the reaction. After 3 h, the reactor was allowed to cool overnight. Liquid products were collected after the autoclave was slowly vented to atmospheric pressure. The spent solid catalyst was filtered and washed repeatedly with acetone before drying in an oven at 80 ºC before further analysis. The liquid products were analysed using a Varian 3800 GC fitted with a DB 5 (5%-phenyl-95%-

dimethylpolysiloxane) capillary column (length, 10 m; internal diameter, 0.53 mm; film thickness, 2.65 µm) and an 8400 auto-sampler. The initial temperature of the column was set at 60 °C. The oven temperature was then ramped up at a rate of 20 °C min^{-1} to 300 °C with a dwelling time of 2 min. The liquid product sample (100 µl) was diluted in 900 µl of toluene and 100 µl of mesitylene solution (0.55 M) acting as an external standard. The isolated components were further validated using a Thermo scientific Trace 1300-Gas Chromatograph equipped with ISQ LT quadrupolar Mass Spectrometer (MS). Acquired mass spectra were compared with the National Institute of Standards and Technology (NIST) mass spectral library.

Results and Discussion

Catalyst characterisation

The textural properties of the synthesised catalysts were characterised by a number of complementary techniques. N_2 porosimetry (**Figure S1a** and **Figure S1b**) demonstrated that both monometallic and bimetallic catalysts exhibit type IV isotherms, characteristic of mesostructured materials. BET analysis of this data shows that the carbon supported metal catalysts possess relatively high surface areas in the range of 450 to 600 m^2 g^{-1} (**Table 1**), in the ballpark of the unmodified carbon support (660 m^2 g^{-1}). Furthermore, the BJH pore size distribution (**Figure S1c** and **Figure S1d**) reveals that all the samples, regardless of the metal type, possess very similar pore diameters of about 3.8 to 3.9 nm (**Table 1**), again consistent with the bare support. Also, as presented in **Table 1**, the elemental analysis confirms that the metal loadings and their respective ratios are similar to those expected. An indication of the particle size for the monometallic samples was obtained from XRD (**Figure 1a** and **Figure 1b**). **Table 1** shows that the pre-reduced Pd, Cu and Ni samples are composed of particles with an average diameter of 4, 5, and 9 nm respectively. However, their size increased after the reduction pre-treatment to 8, 35, and 10 nm for the Pd, Cu and Ni particles, respectively. These values suggest that the Cu catalyst is more prone to sintering under reducing conditions as compared to the Pd and Ni catalysts. The post-reduction metal particle sizes were further studied by TEM (**Figure 2**), which produced results consistent with the XRD estimations (noting for the Cu, one measurement is a number distribution and the other is a volume average). The enlargement of the metal particles is attributed to sintering and agglomeration due to the high temperature reduction treatment and is especially significant for Cu.[23, 24] For the bimetallic particles it was not possible to use the XRD pattern to give a clear estimate of particle size using the above approach, because multiple compositions contribute to the broadening of reflections, as discussed below. However, TEM for each case (**Figure 2**) shows the particle

sizes of the reduced bimetallic catalysts (even the copper containing ones) are consistent with both the size of monometallic Ni and Pd. Previous reports have discussed that these metals do not undergo substantial growth during reduction.[25, 26]

Based on a broad similarity in size, it is often thought a broad similarity in composition will also be present. However, it is instructive in this case to look closely at the XRD patterns and EDS elemental composition mapping of individual metal particles to understand if this is the case, and in turn the implications for catalysis. **Figure 1a** shows the XRD patterns of the Pd-Cu family of catalysts. The diffraction patterns contain a series of sharp reflections attributable to the carbon support (as they appear in all samples), but also broad features typical of nano-sized metal particles. These metallic features in both pure Cu and pure Pd are in the expected positions (allowing for strain or relaxation in the nano-sized particles) for the (111), (200) and (220) of the face-centred cubic (f.c.c.) crystal structure[27] as indicated by the vertical dashed lines. **Figure 1b** shows an expansion around the (111) region for both metals – if the bimetallic particles were homogeneous alloys in the true sense, then it would be expected that Vergard's law would result in a smooth gradual shift in the (111) reflection as a function of composition. This is clearly not the case. Instead as the Cu concentration is increased from pure Pd to $Pd_{60}Cu_{40}$, the main Pd peak is shifted slightly and also a small Cu reflection emerges (at the same 2θ value ~43° as the pure Cu sample). When the concentration is increased still further ($Pd_{40}Cu_{60}$ and $Pd_{20}Cu_{80}$), the same pure Cu reflection becomes substantially stronger and the remaining metal appears to form a wide distribution of different compositions.

This picture is confirmed by STEM-EDS in which the elemental composition fraction of the metal particles (%Cu / total metal) was measured for many individual particles. The results of this are shown in **Figure 1c-e**, where the actual spread of compositions present in each sample determined by EDS can be seen as a histogram. The same trend is seen with a Pd rich alloy present in the $Pd_{60}Cu_{40}$ case, but a high frequency of pure Cu particles in the Cu rich samples. It should be noted that based on the observations from the pure Cu sample it is possible that the Cu particles present are larger and so are observed less frequently by TEM – this is hinted by the XRD where the peak intensity of the Cu reflection changes, but the width is similar from its first appearance on increasing Cu content. The observation of the same general trend by XRD and EDS is valuable, as it excludes the possibility of XRD weak or silent material (e.g. amorphous or disordered particle coatings etc.) being overlooked.

For the Pd-Ni family of catalysts, similar trends can be observed, with **Figure 3a** showing the expected reflections for the Ni f.c.c. phase as denoted by the vertical dashed lines. The expansion in **Figure 3b** around the (111) metallic reflections is however distinct in that Ni is not seen to undergo the same segregational behaviour. Ignoring the sharp reflections from the carbon substrate, with increasing Ni content from Pd_{100} the Pd reflections broaden in $Pd_{60}Ni_{40}$, there is a wide spread of compositions in the $Pd_{40}Ni_{60}$ and then generally Ni rich compositions in the $Pd_{20}Ni_{80}$, but pure Ni doesn't form distinctly separate phases alongside the bimetallic particles. This is again confirmed by EDS (**Figure 3c-e**), which does not show the emergence of high concentrations of pure Ni particles, but relatively broad spreads of composition around the nominal value for all samples.

The chemical environment and oxidation state of the metal surfaces were probed by XPS. The XPS analysis of the monometallic Pd/C material displayed the expected Pd 3d spin–orbit doublet at 335.5 eV and 340.7 eV corresponding to $3d_{5/2}$ and $3d_{3/2}$ respectively, confirming the presence of Pd in the metallic form (**Figure 4a**).[28, 29] It can be observed that as Pd is substituted with Cu in the catalyst, the overall intensity of the Pd 3d signal decreases, as expected. Moreover, there is a small increase in the binding energy of the Pd 3d signals with increasing Cu content, indicating that the Pd in Pd-Cu catalysts was present in a different electronic environment due to the interaction with the Cu (**Figure 4a**). Correspondingly, the Cu 2p signal (**Figure 4b**) shows the expected doublet at 932.8 eV and 952.8 eV (for Cu $2p_{3/2}$ and Cu $2p_{1/2}$ of metallic Cu respectively), and this is seen to shift to a lower binding energy as Pd content increases. It should be noted that a high binding energy shoulder of the main Cu peak and moderate shake-up satellite peaks centred around 942.4 eV and 962.6 eV were detected, suggesting a small amount of oxidic Cu may also be present on the surface,[30] although this could result from handling and sample transfer. The reduction process employed was clearly sufficient for a bulk transformation to yield diffraction by Cu metal (without reflections from Cu_2O or CuO in the XRD pattern). However, the key point is the ~1 eV difference in the binding energies at both Cu and Pd on moving from pure metals to bimetallic samples is strongly indicative of the expected interaction in Pd-Cu particles, consistent with previous literature observations.[31]

Similar to the Pd-Cu catalysts, high resolution Pd 3d XPS of Pd-Ni catalysts exhibit a gradual shift towards higher binding energies, with the largest difference in Pd 3d binding energy observed between $Pd_{20}Ni_{80}$ (Pd $3d_{5/2}$ = 335.8 eV) and pure Pd (Pd $3d_{5/2}$ = 335.5 eV) samples

(**Figure 5a**). As presented in **Figure 5b**, core level spectra of Ni 2p is composed of various oxidation states, including a spin–orbit split doublet at 852.9 eV and 870 eV indicative of metallic Ni, where prominent and broad features are centred at 856.1 eV and 873.7 eV corresponding to Ni in oxidised (NiO), hydroxide ($Ni(OH)_2$) and/or NiOOH forms. Strong satellite peaks were also observed at 861.5 eV and 880 eV.[29, 32] Comparing the pure Ni catalyst with the bimetallic Pd-Ni catalysts, it can be observed that, as expected, the Ni peak intensities decrease with decreasing Ni loading. However, unlike the Pd species, the binding energy of Ni species didn't obviously change with variation in the metal loading, although this could be masked by the presence of different oxidation states in different ratios.

Catalytic reactions

Baseline reference experiments & monometallic catalysts (Pd, Cu & Ni)

The catalytic measurements were conducted in a batch reactor as described in the experimental section. In all cases the reaction was performed for 3 h to ensure that the oleic acid was fully converted. Reference experiments conducted in the absence of metals showed that minimal catalytic activity occurred in the dehydrogenation/deoxygenation system under the reaction conditions employed when a metal catalyst is not present. Three reference experiments were conducted: tetralin dehydrogenation with no catalyst support (activated carbon) or oleic acid as per the scheme in **Figure 6** (conversion 6 %); tetralin dehydrogenation in the presence of the bare carbon support (conversion 8 %); and the tetralin reaction with oleic acid in the presence of the carbon support (conversion 5 % and 4 % for tetralin and oleic acid respectively).

The three monometallic Pd-, Cu- and Ni-based catalysts were tested in tetralin dehydrogenation and oleic acid deoxygenation at 330 °C. **Figure 7** shows the performance of the monometallic Pd, Cu and Ni catalysts in the deoxygenation of oleic acid in tetralin. It is clear that all three metals are active for both tetralin dehydrogenation and oleic acid deoxygenation. It is noteworthy that the oleic acid deoxygenation reported here is a complex reaction, consisting of multiple competing reactions such as decarbonylation, deoxygenation and hydrogenation (**Figure 8**). It is widely accepted that the liberation of hydrogen from the H donor molecule and the hydrogen consumption by the acceptor molecule take place on the same active sites.[33] Tetralin is a compound similar to naphthalene, except that one of its rings is saturated, hence can be dehydrogenated to produce 2 molecules of H_2 (**Figure 8**). Pd shows the highest activity in tetralin conversion (68 %) followed by Cu (47 %) and Ni (33 %) catalysts (**Figure 7**). **Figure S4a** shows the calculated amount of H_2 formed and the maximum amount of H_2 that can be

consumed during the reaction over monometallic catalysts. Pd and Cu were also able to almost completely convert oleic acid (96 % for both catalysts). However, Ni exhibited slightly lower activity in terms of oleic acid conversion with 82 %, as shown in **Figure 7**. It has been reported in the literature that Pd has superior hydrogenation/dehydrogenation and deoxygenation activity than the transition metal based catalysts due to its inherent ability to form surface palladium hydride, which provides an effective catalytic site for hydrogenation/dehydrogenation and deoxygenation reactions.[34, 35]

As **Figure 8** illustrates, according to the literature,[36] in the first step oleic acid can be hydrogenated to form stearic acid using the in situ hydrogen produced by the dehydrogenation of tetralin (**Figure 6**). Stearic acid can follow three different pathways; (i) decarboxylation: stearic acid can lose one CO_2 molecule to form heptadecane ($C_{17}H_{36}$), (ii) decarbonylation which results in the formation of heptadecene ($C_{17}H_{34}$) by eliminating CO and H_2O. Heptadecene ($C_{17}H_{34}$) in turn can be hydrogenated to heptadecane ($C_{17}H_{36}$). (iii) hydrodeoxygenation: by eliminating 2 water molecules and adding 3 hydrogen molecules in two consecutive steps, stearic acid converts into octadecane ($C_{18}H_{38}$). The intermediate stearyl alcohol could also undergo decarbonylation to heptadecane ($C_{17}H_{36}$). **Figure 8** groups the molecules produced based on hydrogen consumption or depth of hydrogenation. The extent of hydrogenation is critically important in understanding the selectivity of the resulting catalysts.

Understanding selectivity differences observed is more complicated. Two factors are at play: (i) the extent of hydrogenation through the reaction network containing sequential hydrogen consuming reactions always starting with stearic acid production as per **Figure 8** (we have already seen hydrogen liberation changes Pd>>Cu>Ni); and (ii) the intrinsic differences in catalysis behaviour over the different metal surfaces. **Figure 7** shows Pd is the only catalyst that has produced a significant amount of octadecane ($C_{18}H_{38}$, 13% selectivity), indicating either that only Pd is active in hydrodeoxygenation of the reactively-formed stearic acid to octadecane or there is insufficient hydrogen available to drive the reaction sequence this far on other metals. Previous studies have suggested in the deoxygenation reaction using Cu and Ni catalysts, C_{18} hydrocarbon products were either absent or negligible (below 1%) due to decarboxylation's or decarbonylation's dominance over hydrodeoxygenation.[37-39] It is clear for both Cu and Ni that the dominant products (steric acid and heptadecene) are those requiring less hydrogen, however their selectivity is not simply in accordance with the availability of hydrogen suggesting Ni has a slightly greater ability to facilitate the

decarbonylation/decarboxylation process. The Ni also produced a higher heptadecane/heptadecene ratio, despite the lower availability of hydrogen consistent with its known catalytic ability in activating hydrogenation of C=C bonds.[24] Heptadecene is nevertheless still present, and this is consistent with the previously reported observations that Ni catalysts favour decarbonylation over decarboxylation.[38, 40] The absence of heptadecene in the Pd catalyst product distribution may be attributed to either the alkene's ease of hydrogenation over the Pd catalyst as soon as it is formed or the formation route *via* decarbonylation being less favourable. These trends in the selectivity are also reflected in the amount of H_2 consumed in the reaction (**Figure S4a**). These observations are important in considering the effectiveness of the different bimetallic catalysts in extending Pd like activity to the Pd diluted bimetallic samples.

Catalysis by $Pd_xCu_{(100-x)}$ and $Pd_xNi_{(100-x)}$ supported bimetallic catalysts

The conversion and selectivity results above are now shown as the end members of the two bimetallic $Pd_xCu_{(100-x)}$ and $Pd_xNi_{(100-x)}$ series in **Figure 9** and **Figure 10** respectively. **Figure S4b** and **Figure S4c** show the amount of hydrogen produced and converted over both series of bimetallic catalysts. The general trends in performance can be rationalised by the structural results obtained from XRD and STEM-EDS and the above discussion on the performance of the individual monometallic catalysts. Firstly, in all cases the consumption of oleic acid is near complete. However, tetralin conversion for the $Pd_xNi_{(100-x)}$ series is diminished going from pure Pd across the bimetallic samples to pure Ni (**Figure 10a**). In the case of the $Pd_xCu_{(100-x)}$ family (**Figure 9a**), the Pd rich $Pd_{60}Cu_{40}$, alike the Ni bimetallics shows a slight decrease in tetralin conversion compared to pure Pd. This decrease in tetralin conversion is much more substantial for the two Cu rich samples. This means that there is a different amount of hydrogen available for reaction with oleic acid in these low tetralin conversion cases. The product distribution is overwhelmingly dominated by mono-hydrogenation products stearic acid and low concentrations of heptadecene (produced by decarbonylation of steric acid without using hydrogen). In contrast all the $Pd_xNi_{(100-x)}$ catalysts produce moderate amounts of heptadecene and octadecane (only seen as very minor products with the $Pd_xCu_{(100-x)}$ series) in addition to more heptadecane and steric acid. This general trend again mirrors the availability of hydrogen (based on tetralin conversions) with more hydrogenated products being present when more hydrogen is available. In the context of the bimetallic systems, it should be noted that hydrogen being liberated over Pd (if this is the more effective site for dehydrogenation) is anticipated from the literature to be able to freely spillover onto other metal sites.[20, 41] The behaviour of

the catalyst with respect to the amount of hydrogen available to react can be rationalised by the structures seen by XRD and STEM-EDS. For the $Pd_{60}Cu_{40}$ and $Pd_{60}Ni_{40}$ in both cases it was seen that composition distribution was that of a Pd rich alloy, with relatively little of the pure base metal being separately detected. This appears to enable much of the reactivity of the Pd to be maintained – consistent also with the small shift in the dominant diffraction peaks. For higher amounts of base metal (the $Pd_{40}Cu_{60}$ and $Pd_{20}Cu_{80}$) there is a segregation of a significant fraction of the Cu (as evidenced by the strong Cu reflection by XRD) and thus a smaller amount of metal remains to form other alloy compositions. The result is there is very likely to be a lower Pd surface area (given the similar size of particles seen by TEM), which fits with the much lower tetralin conversions in these cases. In contrast, the $Pd_{40}Ni_{60}$ and $Pd_{20}Ni_{80}$ are both seen by EDS composition distributions and XRD to exhibit genuine alloy nanoparticles with much less segregation, presumably maximising the number of Pd containing particles. Based on the conversions and selectivities obtained versus pure Ni, the catalytic behaviour of the $Pd_xNi_{(100-x)}$ bimetallic catalysts is more than the simple sum of the two components, even though pure Ni was seen to favour slightly higher rates of further hydrogenation and decarbonylation than Cu in its own right.

In terms of the reaction occurring on the surface, it is useful to keep in mind that the dominant Pd surface species (if large organics such as fatty acid products or naphthalene) may inhibit surface hydrogen formation by competitive adsorption with either tetralin or result in premature desorption of the surface hydrogen prior to reaction.[33] Such competitive effects in transfer hydrogenations more generally have been extensively studied.[42] The presence of a second metal, especially if it causes naphthalene or organic products to bind less strongly, may therefore facilitate access of the hydrogen donor and the reaction of hydrogen with the fatty acid, as well as catalysing the decarbonylation/decarboxylation processes. This tandem effect allows the samples where both metals are homogeneously distributed in each particle to extend the high hydrogenation activity of Pd to lower Pd containing catalysts. Given the higher value of the deeply-hydrogenated products and lower cost of the base metals this points to the attainment of such truly bimetallic materials as a key design requirement for improved transfer hydrogenation / deoxygenation catalysts.

Conclusions

Incipient Wetness Impregnation (IWI) which is a cheap, scalable and commercially used method for catalyst preparation was used to synthesise two different bimetallic catalyst series;

$Pd_xCu_{(100-x)}$ and $Pd_xNi_{(100-x)}$. Materials characterisation by XPS, TEM, STEM-EDS, ICP-OES and XRD show that the IWI approach yields catalysts with varying degrees of Pd-base metal interaction; the $Pd_xCu_{(100-x)}$ series showing more segregation with increasing Cu content than $Pd_xNi_{(100-x)}$. The true bimetallic/alloy particles consistently gave an improved conversion of tetralin and liberation of hydrogen than the materials in which compositional segregation was seen – the $Pd_xNi_{(100-x)}$ series substantially outperforming the $Pd_xCu_{(100-x)}$ catalysts despite the slightly improved tetralin conversion of pure Cu vs pure Ni. In the hydrogen transfer deoxygenation of oleic acid at 330 °C, over 3 h the depth of hydrogenation achieved broadly mirrored the availability of hydrogen (those catalysts better at liberating hydrogen from the hydrogen donor tetralin produced more hydrogenated products), but also exhibited some characteristics of the base metal component, such as decarbonylation to form heptadecane. The $Pd_{60}Cu_{40}$ catalyst exhibited enhanced selectivity toward paraffinic diesel hydrocarbons (C_{17}+C_{18}) in comparison to its monometallic counterparts (Pd & Cu). Overall, this work shows the impact of the structures obtained from standard preparation techniques like IWI when applied to bimetallic systems should be carefully examined as the variations that result can substantially impact performance. It is also demonstrated that, for the hydrogen transfer deoxygenation of oleic acid, Pd like hydrogenation/deoxygenation can be effectively extended by alloying with a cheaper base metal and retain most of the hydrogenation performance as long as a relatively compositional uniform alloy is formed within the catalyst. Oleic acid is a prototypical fatty acid for which deoxygenation is a key step in upgrading biomass to valuable fuels and chemicals, suggesting bimetallic catalysts prepared by a simple, scalable route can be a key approach for reducing the cost of catalysts needed in such processes.

Acknowledgements

This work is part of the collaboration works between Universiti Teknologi PETRONAS, Malaysia and the European Bioenergy Research Institute (EBRI), Aston University, United Kingdom. This work was supported by the Ministry of Higher Education (MOHE) Malaysia through the Long Term Research Grant and Biomass Research Grants. DU GJ Russell Microscopy Facility and Dr Budhika Mendis are gratefully acknowledged for access to TEM and assistance with the STEM-EDS measurements. The British council is acknowledged for funding through the Newton Institutional Links Scheme. GK acknowledges funding from EPSRC (EP/M005186/2). AO and AVB acknowledge funding from the Leverhulme Trust Research Project Grant (RPG-2017-254).

Reference

[1] D. Kubička, P. Šimáček, N. Žilková, Transformation of Vegetable Oils into Hydrocarbons over Mesoporous-Alumina-Supported CoMo Catalysts, Top. Catal., 52 (2009) 161-168.

[2] D. Kubička, L. Kaluža, Deoxygenation of vegetable oils over sulfided Ni, Mo and NiMo catalysts, Appl. Catal., A, 372 (2010) 199-208.

[3] S. Gong, A. Shinozaki, E. W.Qian, Role of Support in Hydrotreatment of Jatropha Oil over Sulfided NiMo Catalysts, Ind. Eng. Chem. Res., 51 (2012) 13953-13960.

[4] L. Jeczmionek, K. Porzycka-Semczuk, Hydrodeoxygenation, decarboxylation and decarbonylation reactions while co-processing vegetable oils over NiMo hydrotreatment catalyst. Part II: Thermal effects – Experimental results, Fuel, 128 (2014) 296-301.

[5] L. Jeczmionek, K. Porzycka-Semczuk, Hydrodeoxygenation, decarboxylation and decarbonylation reactions while co-processing vegetable oils over a NiMo hydrotreatment catalyst. Part I: Thermal effects – Theoretical considerations, Fuel, 131 (2014) 1-5.

[6] H. Zuo, Q. Liu, T. Wang, L. Ma, Q. Zhang, Q. Zhang, Hydrodeoxygenation of Methyl Palmitate over Supported Ni Catalysts for Diesel-Like Fuel Production, Energy Fuels, 26 (2012) 3747-3755.

[7] M. Snåre, I. Kubičková, P. Mäki-Arvela, K. Eränen, D.Y. Murzin, Heterogeneous Catalytic Deoxygenation of Stearic Acid for Production of Biodiesel, Ind. Eng. Chem. Res., 45 (2006) 5708-5715.

[8] M. Arenda, T. Nonnen, W. F.Hoelderich, J. Fischer, J. Groos, Catalytic deoxygenation of oleic acid in continuous gas flow for the production of diesel-like hydrocarbons, Appl. Catal., A., 399 (2011) 198-204.

[9] M. Snåre, I. Kubičková, P. Mäki-Arvela, D. Chichova, K. Eränen, D.Y. Murzin, Catalytic deoxygenation of unsaturated renewable feedstocks for production of diesel fuel hydrocarbons, Fuel, 87 (2008) 933–945.

[10] B.A. Alwan, S.O. Salley, K.Y.S. Ng, Biofuels production from hydrothermal decarboxylation of oleic acid and soybean oil over Ni-based transition metal carbides supported on Al-SBA-15, Appl. Catal., A, 498 (2015) 32-40.

[11] J. Monnier, H. Sulimma, A. Dalai, G. Caravaggio, Hydrodeoxygenation of oleic acid and canola oil over alumina-supported metal nitrides, Appl. Catal., A, 382 (2010) 176-180.

[12] J. Liu, Z. Huang, K. Cai, H. Zhang, Z. Lu, T. Li, Y. Zuo, H. Han, Clean Synthesis of an Economical 3D Nanochain Network of PdCu Alloy with Enhanced Electrocatalytic Performance towards Ethanol Oxidation, Chem. Eur. J., 21 (2015) 17779-17785.

[13] K. Sun, A.R. Wilson, S.T. Thompson, H.H. Lamb, Catalytic Deoxygenation of Octanoic Acid over Supported Palladium: Effects of Particle Size and Alloying with Gold, ACS Catal., 5 (2015) 1939-1948.
[14] J. Zhang, C. Zhao, Development of a Bimetallic Pd-Ni/HZSM-5 Catalyst for the Tandem Limonene Dehydrogenation and Fatty Acid Deoxygenation to Alkanes and Arens for Use as Biojet Fuel, ACS Catal., 6 (2016) 4512-4525.
[15] P.D. Tien, T. Satoh, M. Miura, M. Nomura, Continuous Hydrogen Evolution from Tetrahydronaphthalene over Palladium Catalysts Supported on Activated Carbon Fibers, Energy Fuels, 19 (2005) 2110-2113.
[16] A.M. Robinson, J.E. Hensley, J.W. Medlin, Bifunctional Catalysts for Upgrading of Biomass-Derived Oxygenates: A Review, ACS Catal., 6 (2016) 5026-5043.
[17] H.-W. Lim, M.-J. Park, S.-H. Kang, H.-J. Chae, J.W. Bae, K.-W. Jun, Modeling of the Kinetics for Methanol Synthesis using Cu/ZnO/Al2O3/ZrO2 Catalyst: Influence of Carbon Dioxide during Hydrogenation, Ind. Eng. Chem. Res., 48 (2009) 10448-10455.
[18] I. Hachemi, K. Jenistova, P. Maki-Arvela, N. Kumar, K. Eranen, J. Hemming, D.Y. Murzin, Comparative study of sulfur-free nickel and palladium catalysts in hydrodeoxygenation of different fatty acif feedstock for production of bifuels, Catal. Sci. Technol., 6 (2016) 1476-1487.
[19] K. Jenišťová, I. Hachemi, P. Mäki-Arvela, N. Kumar, M. Peurla, L. Čapek, J. Wärnå, D.Y. Murzin, Hydrodeoxygenation of stearic acid and tall oil fatty acids over Ni-alumina catalysts: Influence of reaction parameters and kinetic modelling, Chem. Eng. J., 316 (2017) 401-409.
[20] G. Kyriakou, M.B. Boucher, A.D. Jewell, E.A. Lewis, T.J. Lawton, A.E. Baber, H.L. Tierney, M. Flytzani-Stephanopoulos, E.C.H. Sykes, Isolated Metal Atom Geometries as a Strategy for Selective Heterogenous Hydrogenations, Science, 335 (2012) 1209 -1212.
[21] A. Thompson, D. Attwood, E. Gullikson, M. Howells, K. Kim, J. Kirz, J. Kortright, I. Lindau, P. Pianetta, A. Robinson, X-Ray Data Booklet, Lawrence Berkeley National Laboratory, Berkeley, CA, 2009.
[22] K.W. Cheah, S. Yusup, G. Kyriakou, M. Ameen, M.J. Taylor, D.J. Nowakowski, A.V. Bridgwater, Y. Uemura, In-situ hydrogen generation from 1,2,3,4-tetrahydronaphthalene for catalytic conversion of oleic acid to diesel fuel hydrocarbons: Parametric studies using Response Surface Methodology approach, International Journal of Hydrogen Energy, (2018).
[23] V. Mukundan, J. Yin, P. Joseph, J. Luo, S. Shan, D.N. Zakharov, C.-J. Zhong, O. Malis, Nanoalloying and phase transformations during thermal treatment of physical mixtures of Pd and Cu nanoparticles, Sci. Technol. Adv. Mater., 15 (2014) 025002.

[24] Z. Zhang, Q. Yang, H. Chen, K. Chen, X. Lu, P. Ouyang, J. Fu, J.G. Chen, In situ hydrogenation and decarboxylation of oleic acid into heptadecane over a Cu–Ni alloy catalyst using methanol as a hydrogen carrier, Green Chem., 20 (2018) 197-205.
[25] J. Mao, Y. Liu, Z. Chen, D. Wang, Y. Li, Bimetallic Pd–Cu nanocrystals and their tunable catalytic properties, Chem. Commun., 50 (2014) 4588-4591.
[26] A.M.D. Yuso, J.L. Meins, Y. Oumellal, V. Paul-Boncour, C. Zlotea, C.M. Ghimbeu, Facile and rapid one pot microwave-assisted synthesis of Pd-Ni magnetic nanoalloys confined in mesoporous carbons, J Nanopart Res, 380 (2016) 18.
[27] D.R. Lide, CRC Handbook of Chemistry and Physics, 86th Edition, Taylor & Francis, 2005.
[28] S. Sitthisa, T. Pham, T. Prasomsri, T. Sooknoi, R.G. Mallinson, D.E. Resasco, Conversion of furfural and 2-methylpentanal on Pd/SiO2 and Pd–Cu/SiO2 catalysts, J. Catal., 280 (2011) 17-27.
[29] Y. Zhao, X. Yang, J. Tian, F. Wang, L. Zhan, Methanol electro-oxidation on Ni@Pd core-shell nanoparticles supported on multi-walled carbon nanotubes in alkaline media, Int. J. Hydrogen Energy, 35 (2010) 3249-3257.
[30] J.P. Espinós, J. Morales, A. Barranco, A. Caballero, J.P. Holgado, A.R. González-Elipe, Interface Effects for Cu, CuO, and Cu2O Deposited on SiO2 and ZrO2. XPS Determination of the Valence State of Copper in Cu/SiO2 and Cu/ZrO2 Catalysts, J. Phys. Chem. B, 106 (2002) 6921-6929.
[31] C. Xu, Y. Liu, J. Wang, H. Geng, H. Qiu, Nanoporous PdCu alloy for formic acid electro-oxidation, J. Power Sources, 199 (2012) 124-131.
[32] M.S. Ahmed, S. Jeon, Synthesis and electrocatalytic activity evaluation of nanoflower shaped Ni-Pd on alcohol oxidation reaction, J. Electrochem. Soc., 161 (2014) F1300-F1306.
[33] H. Shafaghat, P.S. Rezaei, W.M.A. Wan Daud, Using decalin and tetralin as hydrogen source for transfer hydrogenation of renewable lignin-derived phenolics over activated carbon supported Pd and Pt catalysts, Journal of the Taiwan Institute of Chemical Engineers, 65 (2016) 91-100.
[34] T. Morgan, D. Grubb, E. Santillan-Jimenez, M. Crocker, Conversion of Triglycerides to Hydrocarbons over Supported Metal Catalysts, Top. Catal., 53 (2010) 820-829.
[35] I. Simakova, O. Simakova, P. Maki-Arvela, A. Simakov, M. Estrada, D.Y. Murzin, Deoxygenation of palmitic and stearic acid over supported Pd catalysts: Effect of metal dispersion., Appl. Catal., A, 355 (2009) 100-108.

[36] Y. Yang, Q. Wang, H. Chen, X. Zhang, Enhancing selective hydroconversion of C18 fatty acids into hydrocarbons by hydrogen-donors, Fuel, 133 (2014) 241-244.
[37] J.A. Botas, D.P. Serrano, A. Garcia, D. Vicente, D. Ramos, Catalytic conversion of rapeseed oil into raw chemicals and fuels over Ni- and Mo- Modified nanocrystalline ZSM-5 zeolite, Cat. Today, 195 (2012) 59-70.
[38] T. Morgan, E. Santillan-Jimenez, A.E. Harman-Ware, Y. Ji, D. Grubb, M. Crocker, Catalytic Deoxygenation of Triglycerides to Hydrocarbons over Supported Nickel Catalysts, Chem. Eng. J., 189-190 (2012) 346-355.
[39] E. Santillan-Jimenez, T. Morgan, J. Shoup, A.E. Harman-Ware, M. Crocker, Catalytic deoxygenation of triglycerides and fatty acids to hydrocarbons over Ni-Al layered double hydroxide, Catal. Today, 237 (2014) 136-144.
[40] B. Peng, C. Zhao, S. Kasakov, S. Foraita, J.A. Lercher, Manipulating catalytic pathways: deoxygenation of palmitic acid on multifunctional catalysts, Chem. Eur. J., 19 (2013) 4732-4741.
[41] G. Kyriakou, E.R.M. Davidson, G. Peng, L.T. Roling, S. Singh, M.B. Boucher, M.D. Marcinkowski, M. Mavrikakis, A. Michaelides, E.C.H. Sykes, Significant Quantum Effects in Hydrogen Activation, ACS Nano., 8 (2014) 4827-4835.
[42] R.A. Johnstone, A.H. Wilby, I.D. Entwistle, Heterogeneous catalytic transfer hydrogenation and its relation to other methods for reduction of organic compounds, Chem. Rev., 85 (1985) 129-170.

FIGURE 1

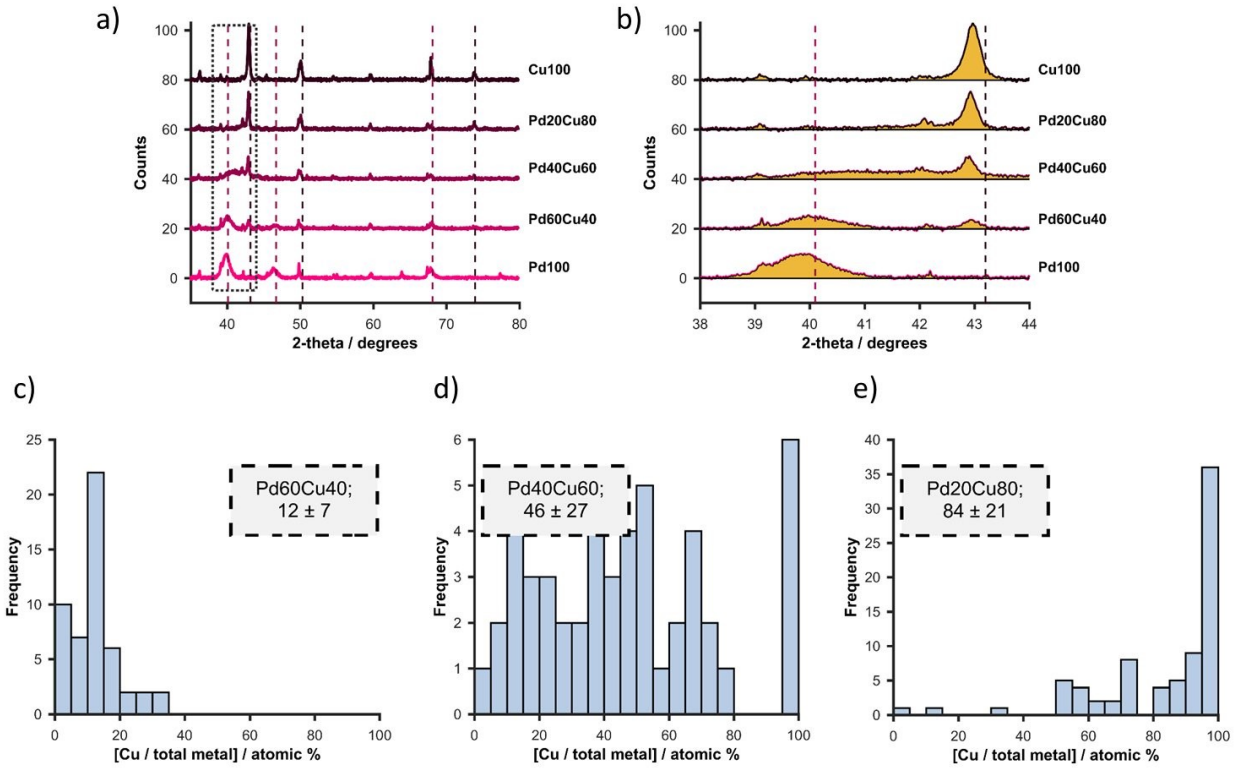

Figure 1. XRD patterns of Pd_{100}, $Pd_{60}Cu_{40}$, $Pd40_{Cu60}$, $Pd_{20}Cu_{80}$ and Cu_{100} supported on activated carbon after reduction and EDS composition distributions for the bimetallic samples (a) wide scan XRD, vertical dashed lines denote the position of reflections in the bulk metals (Pd, pink; Cu, black) and (b) expanded region of XRD pattern around (111) reflections of the two metals, shown by dotted rectangle in 'a'. (c), (d) and (e) composition distributions derived from EDS analysis of multiple individual metal particles in each catalyst

.

FIGURE 2

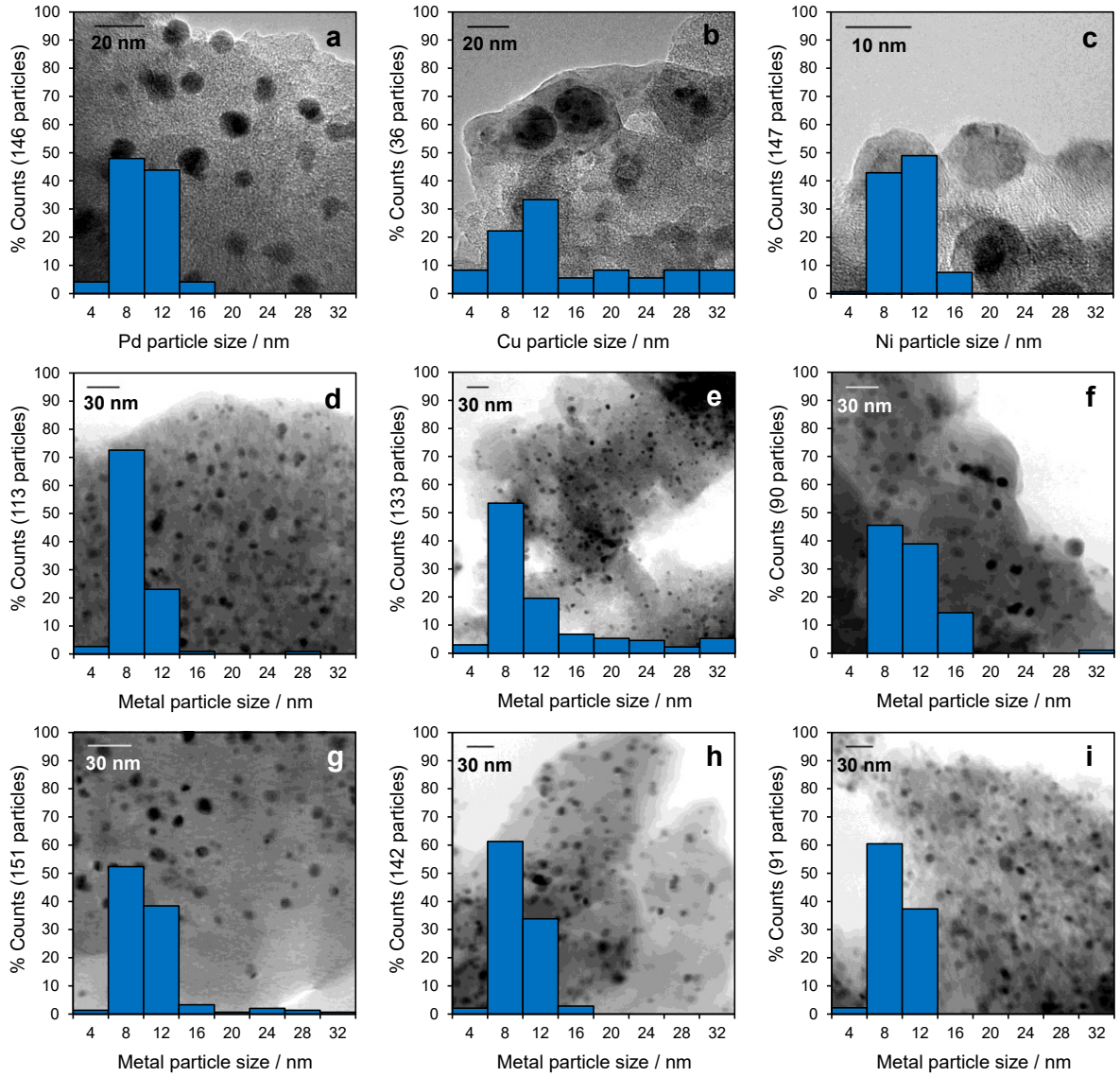

Figure 2. Bright field transmission electron micrographs of 5 wt. % (a) Pd, (b) Cu, (c) Ni, (d) Pd-Cu ($Pd_{60}Cu_{40}$), (e) Pd-Cu ($Pd_{40}Cu_{60}$), (f) Pd-Cu ($Pd_{20}Cu_{80}$), (g) Pd-Ni ($Pd_{60}Ni_{40}$), (h) Pd-Ni ($Pd_{40}Ni_{60}$) and (i) Pd-Ni ($Pd_{20}Ni_{80}$) on activated carbon after reduction and their corresponding particle size distribution.

FIGURE 3

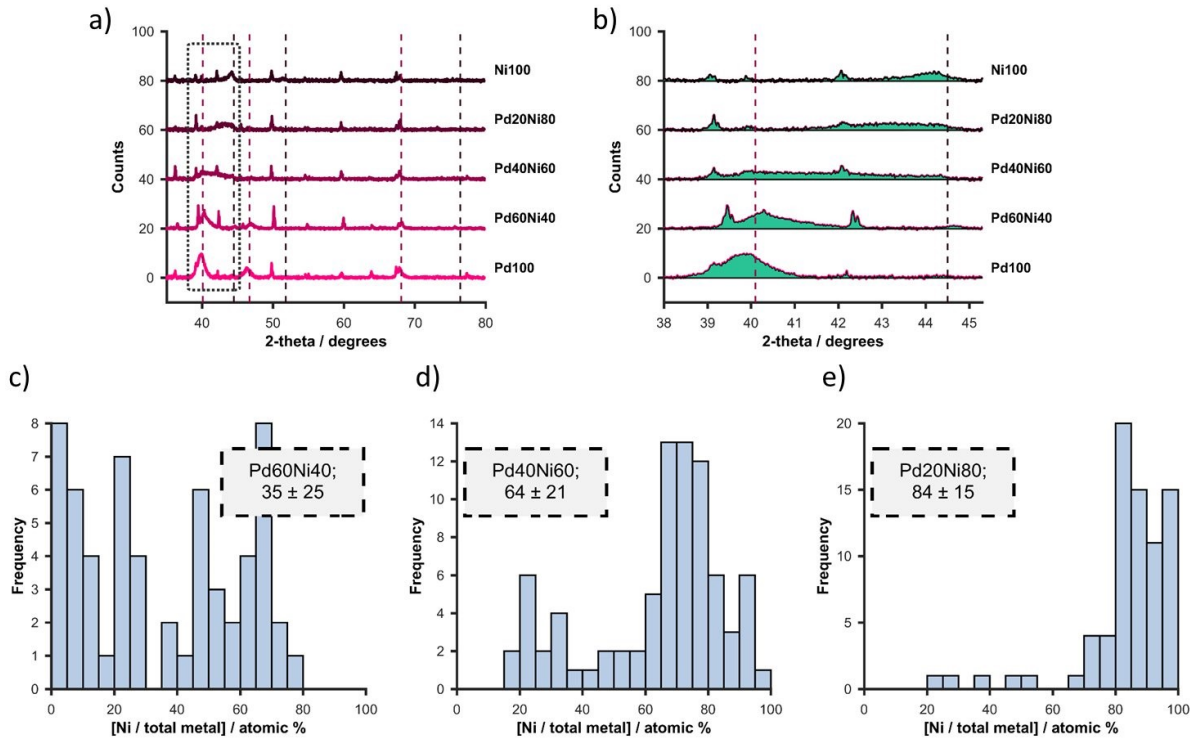

Figure 3. XRD patterns of Pd_{100}, $Pd_{60}Ni_{40}$, $Pd_{40}Ni_{60}$, $Pd_{20}Ni_{80}$ and Ni_{100} supported on activated carbon after reduction and EDS composition distributions for the bimetallic samples. (a) Wide scan XRD, vertical dashed lines denote the position of reflections in the bulk metals (Pd, pink; Ni, black), (b) expanded region of XRD pattern around (111) reflections of the two metals, shown by dotted rectangle in 'a'. (c), (d) and (e) composition distributions derived from EDS analysis of multiple individual metal particles in each catalyst.

FIGURE 4

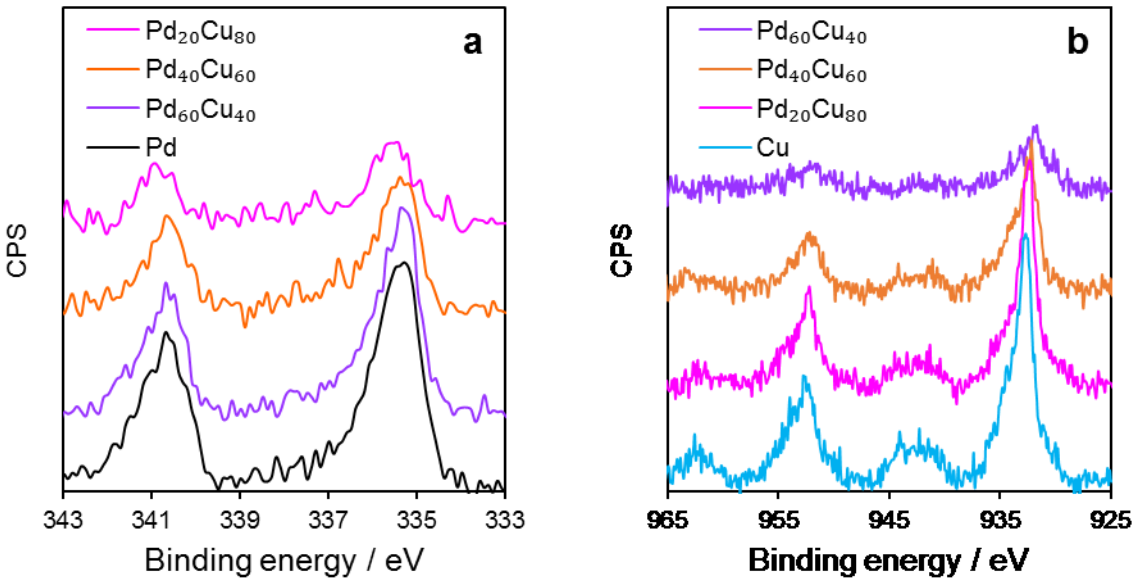

Figure 4. XPS of Pd 3d (a) and Cu 2p (b) for the Pd, Cu and Pd-Cu materials supported on activated carbon after reduction pre-treatment.

FIGURE 5

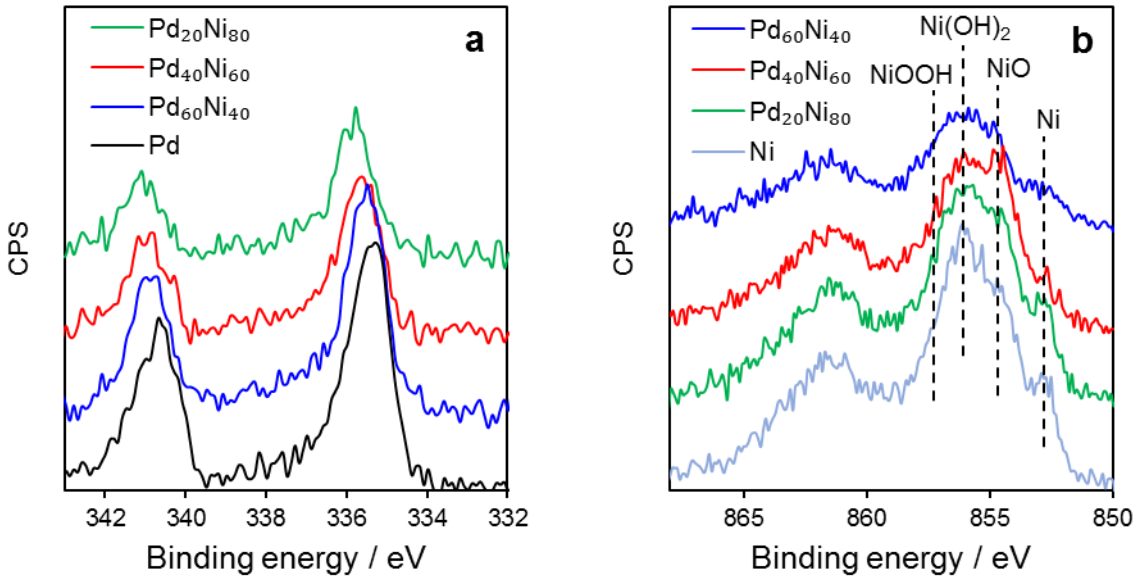

Figure 5. XPS of Pd 3d (a) and Ni 2p (b) for the Pd, Ni and Pd-Ni materials supported on activated carbon after reduction pre-treatment.

FIGURE 6

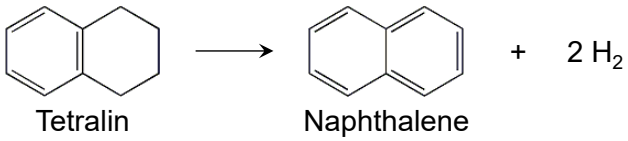

Figure 6. Tetralin dehydrogenation reaction.

FIGURE 7

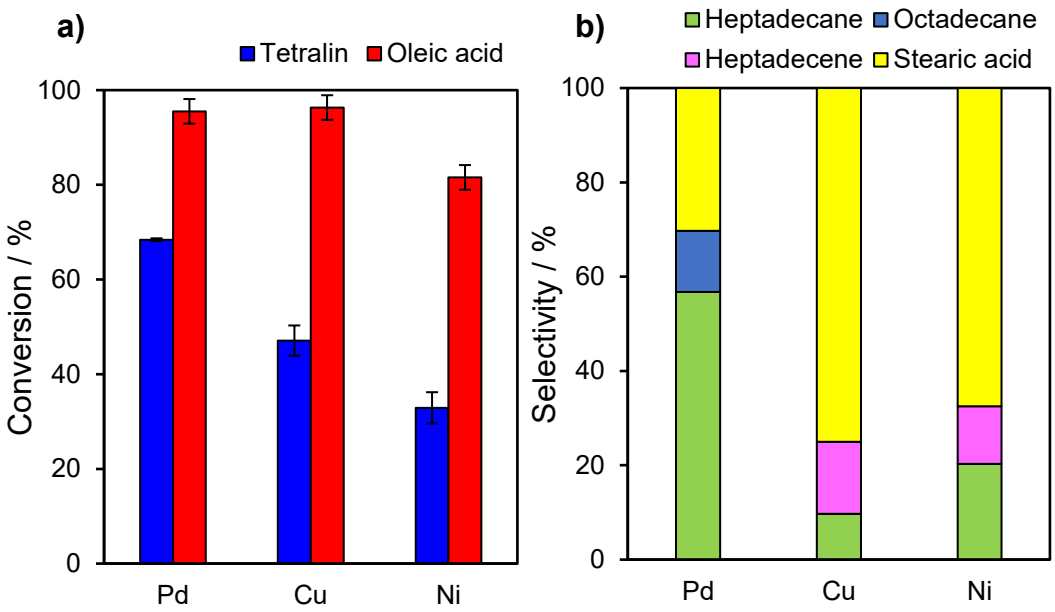

Figure 7. a) Conversion of tetralin and oleic acid and b) selectivity of products in oleic acid deoxygenation using tetralin as hydrogen source over monometallic carbon supported Pd, Cu and Ni catalysts. Reaction conditions: 1 ml of oleic acid, 1 ml of tetralin, 50 mg of catalysts, 330 °C, 10 bar of N_2, 3 h and 1100 rpm stirring.

FIGURE 8

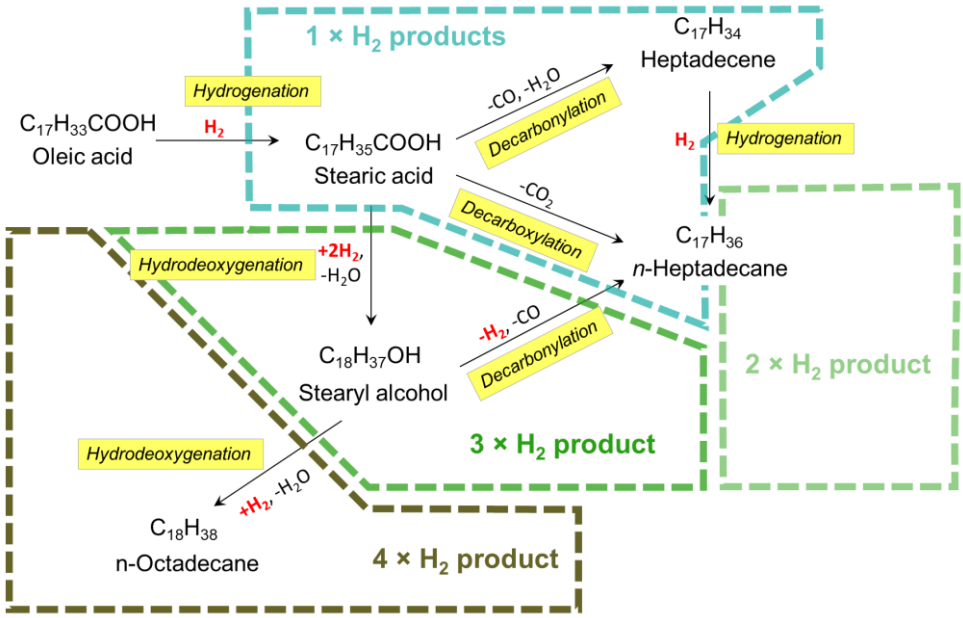

Figure 8. Reaction pathway for deoxygenation of oleic acid in presence of H_2.

FIGURE 9

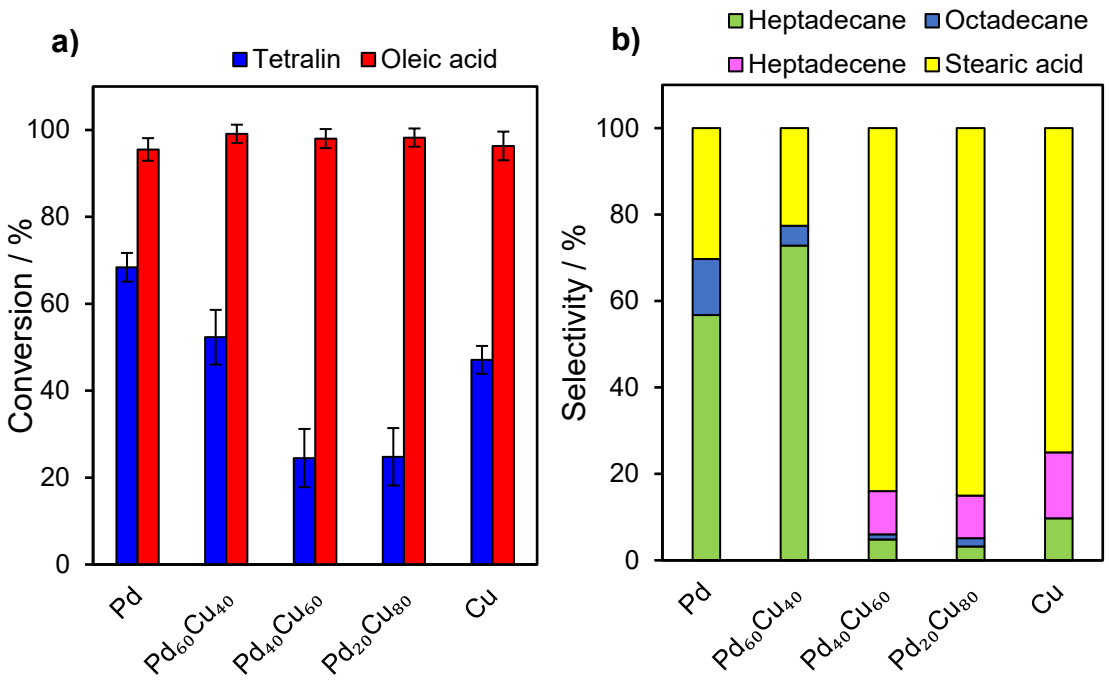

Figure 9. a) Oleic acid conversion in tetralin dehydrogenation over $Pd_xCu_{(100-x)}$ catalyst series with x = 0, 20, 40, 60 and 100. b) Liquid product selectivity/distribution of oleic acid conversion in tetralin. Reaction conditions: 1 ml of oleic acid, 1 ml of tetralin, 50 mg of catalysts, 330 °C, 10 bar of N_2 and 1100 rpm.

FIGRUE 10

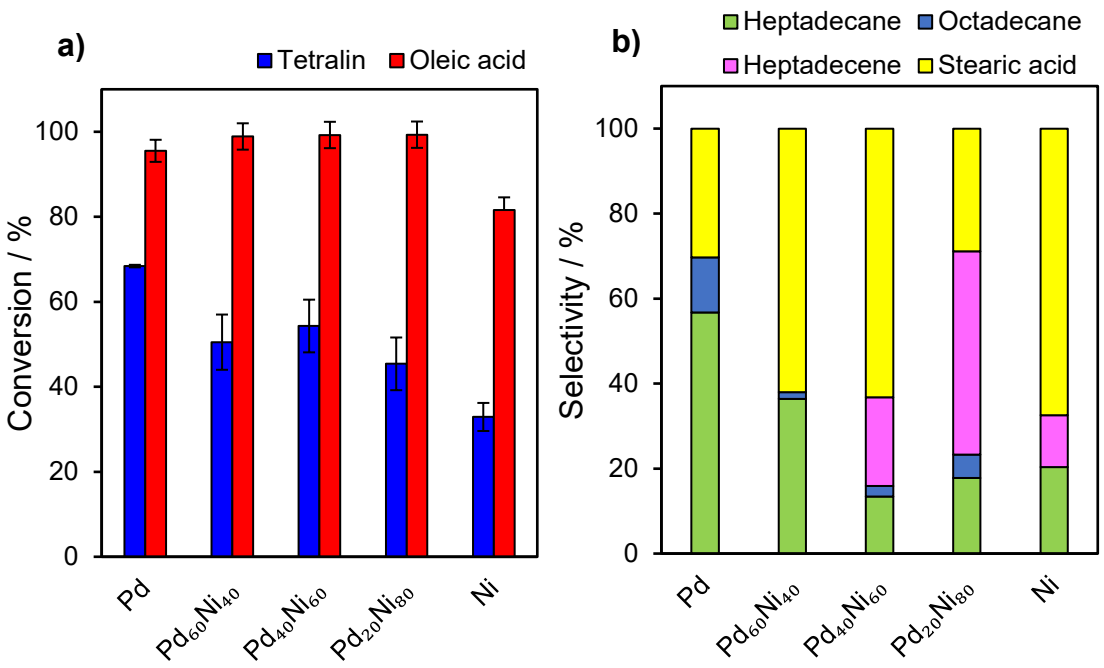

Figure 10. a) Oleic acid conversion in tetralin dehydrogenation over $Pd_xNi_{(100-x)}$ catalyst series with x = 0, 60, 40, 20 and 100. b) Liquid product selectivity/distribution of oleic acid conversion in tetralin. Reaction conditions: 1 ml of oleic acid, 1 ml of tetralin, 50 mg of catalysts, 330 °C, 10 bar of N_2 and 1100 rpm.

TABLE 1

Table 1. Textural properties of monometallic and bimetallic catalyst samples.

Type of catalysts	Nominal molar ratio (Pd:Cu/Ni)	Metal loading[a]/ wt.%				Surface area[b] / m^2 g^{-1}	Pore diameter[c] / nm	Crystallite size[d] / nm		TEM particle size / nm
		Pd	Cu	Ni	Total			Pre-reduction	Post -reduction[e]	
Norit Carbon	-	-	-	-	-	660	4.0	-	-	-
Pd	1:0	4.8	-	-	4.8	535	3.8	4	8	8.0
Cu	0:1	-	3.6	-	3.6	547	3.8	5	35	17.3
Ni	0:1	-	-	4.9	4.9	562	3.9	9	10	8.5
$Pd_{60}Cu_{40}$	3:2	3.1	1.2	-	4.4	596	3.9	-	-	8.1
$Pd_{40}Cu_{60}$	2:3	2.5	2.2	-	4.6	450	3.8.	-	-	10.6
$Pd_{20}Cu_{80}$	1:4	1.3	3.3	-	4.5	580	3.8	-	-	8.9
$Pd_{60}Ni_{40}$	3:2	3.3	-	1.2	4.5	575	3.9	-	-	8.0
$Pd_{40}Ni_{60}$	2:3	2.3	-	2.0	4.3	572	3.9	-	-	7.7
$Pd_{20}Ni_{80}$	1:4	1.4		2.9	4.3	517	3.8	-	-	7.6

[a] ICP-OES, [b] BET, [c] BJH, [d] XRD and [e] Reduction of the catalysts was conducted at 450 °C for 2 h.